

Raman vibrational spectra of bulk to monolayer ReS₂ with lower symmetry

Yanqing Feng^{1}, Wei Zhou^{1*}, Yaojia Wang¹, Jian Zhou², Erfu Liu¹, Yajun Fu¹, Zhenhua Ni³,
Xinglong Wu¹, Hongtao Yuan^{4,5}, Feng Miao¹, Baigeng Wang¹, Xiangang Wan¹ & Dingyu Xing¹*

¹ National Laboratory of Solid State Microstructures, School of Physics, Collaborative
Innovation Center of Advanced Microstructures, Nanjing University, Nanjing 210093, China.

² Department of Materials Science and Engineering, Nanjing University, Nanjing 210093, China.

³ Department of Physics, Southeast University, Nanjing 211189, China.

⁴ Geballe Laboratory for Advanced Materials, Stanford University, Stanford, California 94305,
USA

⁵ Stanford Institute for Materials and Energy Sciences, SLAC National Accelerator Laboratory,
Menlo Park, California 94025, USA

KEYWORDS:

ReS₂, Raman spectra, local density approximation, two-dimensional layered materials

ABSTRACT

Lattice structure and symmetry of two-dimensional (2D) layered materials are of key importance to their fundamental mechanical, thermal, electronic, and optical properties. Raman spectroscopy, as a convenient and nondestructive tool, however has its limitations on identifying all symmetry allowing Raman modes and determining the corresponding crystal structure of 2D layered materials with high symmetry like graphene and MoS₂. Due to lower structural symmetry and extraordinary weak interlayer coupling of ReS₂, we successfully identified all 18 first-order Raman active modes for bulk and monolayer ReS₂. Our local density approximation (LDA) calculations perfectly reproduce all the Raman modes unexpectedly without any van der Waals (vdW) correction, verifying no surface reconstruction effect and the absence of low frequency rigid-layer Raman modes below 100 cm⁻¹. Combining with Raman and LDA thus provides a general approach for studying the vibrational and structural properties of 2D layered materials with lower symmetry.

2D layered materials have attracted a large amount of research interest due to their rich physics and tremendous application potentials.¹⁻³ As a nondestructive and powerful technique for characterizing Brillion zone center (Γ point) phonon properties of materials, Raman spectroscopy yields information about the structure, lattice symmetry, crystal quality and the existence of defects and impurities⁴⁻⁷. It has also been widely used to understand the electronic and vibrational properties, as well as their dependence on the thickness of various 2D layered materials.⁸⁻¹² While lattice symmetry plays a crucial role in determining their fundamental properties, most experimentally-investigated 2D layered materials have high lattice symmetry, such as graphene and MoS₂. For these materials, usually there are low-frequency rigid-layer Raman active modes below 100 cm⁻¹ in the few-layer and bulk samples due to stacking structure. These modes have very weak intensity, which brings huge challenge for traditional Raman spectroscopy to experimentally identify all the symmetry allowing Raman active peaks given the strong Rayleigh scattering. For example, the crystalline structure of bulk MoS₂ belongs to the D_{6h}^4 space group and has two S-Mo-S single layers with four Raman active modes, namely E_{1g} , A_{1g} , E_{2g}^1 , and E_{2g}^2 modes.¹³⁻¹⁴ Among these modes, the double-degenerate shear mode (E_{2g}^2 mode) is almost negligible due to strong Rayleigh scattering.¹² In contrast, 2D layered material ReS₂ was recently found¹⁵ to have very weak interlayer coupling and quite low symmetry (the symmetry space group $P\bar{1}-C_i^1$ ¹⁵⁻¹⁸) with triclinic lattice structure. It owns only one single layer in the bulk unit cell, which may bring novel and intriguing vibrational properties in Raman spectra.

In this article, we systematically studied the Raman spectra of bulk to monolayer ReS₂ samples. Due to the one single layer structure in bulk ReS₂, ReS₂ shows no low frequency (below 100 cm⁻¹) rigid-layer vibration Raman modes, sharply contrary to other well-known

members of transition metal dichalcogenides (TMDs with the chemical formula MX_2 , M: transition metal element, X: chalcogen element). Combining with LDA calculations, we successfully identified all 18 symmetry allowing first-order Raman active peaks for bulk and monolayer ReS_2 in experiment. From monolayer to bulk, we observed that only two (the first A_g -like and sixteenth cp mode) of Raman modes exhibit measurably ($\sim 1.0 \text{ cm}^{-1}$) thickness induced frequency shifts, while many other modes have tiny (0.5 or 0.6 cm^{-1}) shifts. Such results verify the very weak interlayer interaction and no surface reconstruction in this layered material. The excellent agreement between the theoretical and experimental Raman results points to such approach as a power tool to characterize vibrational and structural properties of 2D layered materials with low symmetry.

Few-layer ReS_2 flakes were prepared from the bulk ReS_2 crystal (2D semiconductors) through mechanical exfoliation method to silicon substrates covered by 300 nm SiO_2 layer. Similar to graphene, thin ReS_2 flakes and their number of layers can be first identified by visual color differences between samples and substrates under an optical microscope. In FIG.1(a), an optical image of a typical single-layer ReS_2 flake was shown. Its thickness was determined to be 0.87 nm by an atomic force microscopy (AFM) in the ScanAsyst mode (insert of FIG.1(b)). Since the interlayer distance of ReS_2 is 0.62 nm, we can thus confirm it is a monolayer flake.

Bulk ReS_2 crystallizes in a triclinic structure with the space group $P\bar{1}-C^1_i$ (No. 2)¹⁵⁻¹⁸. As shown in FIG.1(c), this structure can be thought as a distorted 1T- MX_2 dichalcogenides, and the only symmetry operation for this material is the inversion with center located in the middle of Re1-Re3 bond. We started with optimizing the lattice structure. The numerical lattice parameter and independent internal atomic coordinates for bulk ReS_2 , as well as the experimentally obtained results¹⁶, were listed in TABLE I. We find that the standard LDA method successfully

reproduces the internal coordinates and only underestimates the lattice constants slightly. For example, it underestimates the interlayer parameter a for about 1.6%, while the generalized gradient approximation (GGA) scheme significantly overestimates the same parameter for about 15.1%. The vdW-corrected (vdW-DFT) method gives a smaller interlayer lattice constant than the LDA and the experimental value. We thus conclude that the standard LDA method can well reproduce the interlayer lattice constant without any vdW correction, which is due to weak interlayer vdW interaction in this layered material.¹⁵ Same to the common MX₂ dichalcogenides^{12,19-24}, each Re of ReS₂ has six neighboring S sites, but the lattice is distorted and the Re-S bond lengths are no longer equal to each other. For example, the Re1 site bonds with S1, S2, S3, S4, S5, and S7, and the LDA bond lengths are 2.33, 2.36, 2.44, 2.40, 2.34 and 2.42 Å, respectively, and Re2-Si (i=1, 2, 3, 4, 6, 8) bond distances are 2.34, 2.46, 2.40, 2.38, 2.31 and 2.51 Å, respectively. But the average lengths are approximately the same for the two independent Re-S bonds (2.38 Å for Re1-S and 2.39 Å for Re2-S), which are shorter than Mo-S bond in MoS₂ (2.42 Å²⁰). Furthermore, unlike common MX₂ dichalcogenides in which metal-metal bonds are non-existent^{12,19-24}, in ReS₂ each Re atom has three neighboring Re sites. There are four Re atoms in the unit cell participating in bonding and forming a parallelogram-shaped Re₄ cluster. But the Re atoms at longer diagonal sites (Re2, Re4) in the parallelogram-shaped Re₄ cluster do not bond as shown in the FIG.1(c). The Re-Re bonding lengths are listed in TABLE II (Similarly, the LDA and vdW-DFT underestimate the Re-Re bonds while the GGA overestimates Re-Re bonds a bit). This forming of Re₄ cluster brings significant amount of bond charges between the Re-Re dimers.¹⁵ Thus different S atoms have completely different environment and span different Re-Re bonds number: S1 spans three metal-metal bonded Re atoms (Re1-Re2, Re1-Re3 and Re2-Re3); S2 and S4 span a single metal-metal bond (Re1-Re4

for S2, Re1-Re2 for S4); and S3 is a little isolated and spans no metal-metal bonds as shown in FIG.1(c). Meanwhile, the forming of Re4 cluster leads to a single layer structure per unit cell, which is quite different from the common MX₂ dichalcogenides, such as 1T-MX₂²¹, 2H-MX₂^{12,22} and 3R-MX₂^{23,24}.

We first performed the non-resonance Raman scattering measurements on bulk ReS₂, with results shown in FIG.2(a). Our experiments (Horiba-JY T64000) were carried out at ambient conditions in the backscattering geometry. The incident laser wavelength is 633 nm within the 0.6 cm⁻¹ resolution and power is less than 1 mW to minimize laser heating. For a 120 s spectrum collection time, main Raman features were clearly recorded followed by typical Lorentzian fittings which give the Raman shift values. Due to the limitation of spectrometer, we only measured Raman modes above 100 cm⁻¹ in FIG.2(a). The strong peak located at 520.7 cm⁻¹ comes from silicon substrate. Similar to the results of Tongay et al.¹⁵, we also found that there are two big Raman peaks located around 150 cm⁻¹ and 200 cm⁻¹. By carefully collecting the signals, we eventually observed 18 modes spreading in 100-450 cm⁻¹ range. We marked these observable Raman active modes by the arrows in FIG.2(a), and listed their frequencies in TABLE III.

There are 12 atoms in the unit cell, thus bulk ReS₂ possesses 36 vibration modes. ReS₂ is isomorphic to the point group C_i (the Schoenflies character tables for the point groups can be found in Ref.²⁵), and according to decomposition²⁶ and group theory symmetry analysis, the irreducible representations of the 36 Γ point phonon modes can be written as $\Gamma=18(A_g + A_u)$. There are 18 asymmetric A_u modes and 18 symmetric A_g modes with respect to inversion. Three acoustical modes and infrared active optical modes must be asymmetric under inversion. Thus 15 infrared active and 18 Raman modes can be found in bulk ReS₂. It is worth to note that for ReS₂

all of the Raman active and infrared active modes are non-degenerate. While for the common MX_2 dichalcogenides, such as 2H-MoS_2 , there exist two-degenerate E symmetry in-plane vibration modes (E^1_{2g} and E^2_{2g})^{12,13} besides the non-degenerate A_g modes due to high symmetric lattice structure.

To further answer the questions that whether there are first-order Raman modes located below 100 cm^{-1} and whether 18 observed Raman modes above 100 cm^{-1} are all first-order modes, we performed LDA, vdW-DFT and GGA calculations based on our optimized structure, and presented the numerical frequencies of the 18 A_g modes in TABLE III. It is found that both the LDA and vdW-DFT methods calculated frequencies perfectly agree with experimental results. The maximal discrepancy between the LDA and experimental data is only 5.4 cm^{-1} and most of the differences are less than 2.0 cm^{-1} . Thus we believe that the standard LDA without considering the vdW interaction is already sufficiently to describe the geometric structure and the mechanical properties for this weakly interlayer coupled layered material. For other layered materials such as graphite^{10,27}, h-BN^{28,29} and MoS_2 ^{12,19,20}, the LDA has quite successfully reproduced the geometry and given reasonable results for the phonon modes. Tan et al.¹⁰ and Luo et al.²⁰ also confirmed that the LDA predicts the same correct interlayer spacing to vdW-DFT and thus reproduces good Raman frequencies matching with the experimental results in their respective calculations. Thus, we believe that standard LDA without considering the vdW interaction does provide the change in force with respect to ionic displacements, the force constants and phonon frequencies for the 2D systems. On the other hand, the GGA calculations considerably underestimate the Raman frequencies as shown in TABLE III. From here onward, we focus on the LDA results.

Since all the calculated A_g modes frequencies agree with the experimental data very well, we conclude that the 18 experimental peaks, marked in FIG.2(a) and listed in TABLE III, are the 18 symmetry allowing first-order Raman modes. There are no Raman active vibrations below 100 cm^{-1} . As discussed above, ReS_2 has no low frequency rigid-layer shear Raman vibration modes due to the fact that the Re atoms form the Re_4 cluster, and consequently the unit cell of bulk ReS_2 has only one layer. For some MX_2 dichalcogenides which have distorted 1T structure, such as ReSe_2 ³⁰ and TcS_2 ³⁰, the low frequency rigid-layer shear Raman modes should be also absent. While for those layered compounds whose unit cells have two layers, the low frequency E_{2g} rigid-layer shear Raman vibration modes exist. Some examples include the modes of about 42 cm^{-1} for graphite^{10,31}, about 52 cm^{-1} in bulk h-BN^{29,32}, about 32 cm^{-1} in bulk MoS_2 ^{12,14}, and 22 cm^{-1} in bulk WSe_2 ¹².

By checking the phonon eigenvectors, we now can analyze the Raman modes. We denote the one with large out-of-plane vibration weights as A_g -like mode, with large in-plane vibration weights as E_g -like mode and with both strong in-plane and out-of-plane vibration weights as cp mode. Our numerical results show that from low frequency to high frequency, the vibration weights of S atoms increase and Re atoms decrease gradually. As shown in TABLE III, there are four A_g -like modes. Two low frequency A_g -like modes ($136.8, 144.5\text{ cm}^{-1}$) mainly involve the out-of-plane vibrations of Re atoms, and the high frequency A_g -like modes ($422.3, 443.4\text{ cm}^{-1}$) mainly involve the out-of-plane vibrations of S atoms. The E_g -like modes, located at $153.6, 163.4, 218.2, 238.1\text{ cm}^{-1}$, mainly involve in-plane vibrations of Re atoms; while other two E_g -like modes, at $308.5, 312.1\text{ cm}^{-1}$, are mainly in-plane vibrations of S atoms. These frequency distributions of E_g -like modes are similar to the results reported by Tongay et al.¹⁵, except one E_g -like Raman mode at 218.2 cm^{-1} (213 cm^{-1} in the Raman spectrum of Tongay et al.¹⁵, which

was treated as A_g -like mode with mostly out-of-plane vibrations). The cp modes at 275.1 and 282.6 cm^{-1} involve in-plane and out-of-plane vibrations of Re and S atoms; while the cp modes above 300 cm^{-1} are mainly in-plane and out-of-plane vibrations of S atoms.

We also schematically showed several typical vibration modes in FIG.3. The E_g -like mode at 153.6 cm^{-1} mainly involves in-plane stretching vibrations of Re-Re bonds along the edge of the parallelogram-shaped clustering of the Re₄ unit, and in-plane vibrations of a pair of S atoms (S1 and S5) atoms as well. The E_g -like modes at 163.4, 218.2 cm^{-1} involve in-plane stretching vibrations of Re-Re bonds, and the vibrations of the pair of S atoms which span only one metal-metal bond. The E_g -like mode at 238.1 cm^{-1} vibrates mainly along the diagonal line of the parallelogram-shaped clustering of the Re₄ unit with little S atoms vibrations. As discussed above, different S atoms span different Re-Re environment, and thus their vibrations bring different amount of bond charge polarizability between the Re-Re dimers, thus different Raman intensity. Hence, E_g -like modes at 153.6, 163.4, 218.2 cm^{-1} peak strong Raman peaks in Raman spectrum shown in FIG.2(a). And the mode of 153.6 cm^{-1} peaks the strongest. A_g -like mode at 144.5 cm^{-1} also peaks relatively strong Raman peak in FIG.2(b) due to the participation of the pair of S1 and S5 atoms in-plane stretching vibrations, while A_g -like mode at 136.8 cm^{-1} does not involve S atoms vibrations peaking quite weakly.

Since Raman spectroscopy is also a powerful tool to study layer number dependent properties of 2D layered materials^{6,8,9}, here we also studied the Raman spectra of few- and monolayer ReS₂ systems. While the presence of inversion symmetry for MoS₂ depends on its layer number.^{13,19,22}, the few-layer ReS₂ flakes always have the inversion symmetry regardless the layer number is even or odd. We performed structural optimization and listed the numerical results for monolayer ReS₂ in TABLE IV. To the best of our knowledge, there is no experimental

measurement on the lattice parameters for monolayer ReS₂, we thus listed the previous theoretical data for comparison.^{15,33} Our numerical results agree well with the previous theoretical results. As shown in TABLE I and TABLE IV, the differences between the numerical results of bulk and monolayer ReS₂ are quite small, confirming the interlayer interaction is indeed very weak.

The Raman spectrum of monolayer ReS₂ was shown in FIG.2(b) and the observable Raman active peaks were marked in arrows. The monolayer ReS₂ shows very similar Raman spectrum to that of bulk one, with exact 18 observable Raman active modes in the 100-450 cm⁻¹ range. We listed the concrete frequencies in TABLE III. We do not find any new peaks, confirming that the symmetry is remained from bulk to monolayer. Thus the group of Γ point of monolayer ReS₂ is still isomorphic to the point group C_{3i}. $\Gamma=18(A_g + A_u)$. Our DFT calculations confirm 18 non-degenerate first-order Raman active modes in monolayer ReS₂ in TABLE III. We observed that among all 18 modes, both our experimental results and the theoretical calculations show that the first A_g-like mode exhibits an obvious red shift as the thickness decreases from bulk to monolayer. It softens by 1.1 cm⁻¹ (from 140.3 cm⁻¹ to 139.2 cm⁻¹) experimentally and 4.1 cm⁻¹ (from 136.8 cm⁻¹ to 132.7 cm⁻¹) theoretically as shown in TABLE III. The sixteenth cp mode presents a 1.0 cm⁻¹ blue shift experimentally (from 407.3 cm⁻¹ to 408.3 cm⁻¹) and a 2.1 cm⁻¹ (from 408.7 cm⁻¹ to 410.8 cm⁻¹) blue shift theoretically. Many other modes have tiny (0.5 or 0.6 cm⁻¹) thickness induced frequency shifts, suggesting the very weak interlayer interaction in this layered material, and the absence of discernible surface reconstruction. In contrast, in MoS₂ systems, the surface reconstruction³⁴ softens the A_g mode of the topmost layer by 25 cm⁻¹¹⁸ due to strong interlayer interaction.

We next conducted a systematic Raman spectra study of few-layer labeling as NL (N is the layer number = 2, 3, 4 here) ReS₂ flakes, which were also shown in FIG.2(b). It shows similar Raman spectra to that of bulk and monolayer ReS₂, with 18 corresponding observable Raman active modes in the 100-450 cm⁻¹ range. As the layer number N increases, there should be 18N non-degenerate first-order Raman modes from the group theory analysis. $\Gamma=18N(A_g + A_u)$. But the differences of the Raman modes between NL (N ≥ 2) and monolayer are tiny, further confirming the ultra-weak interlayer interaction. Meanwhile, from bulk to monolayer, we do not notice any regular and distinct thickness dependent tendency of the line widths and the peak intensity of all the 18 Raman active peaks.

In conclusion, we presented both DFT and experimental Raman scattering studies on lattice vibrations of bulk to monolayer ReS₂, which is a 2D TMD material with low lattice symmetry. Combining with LDA calculations, we successfully identified all symmetry allowing Raman modes for both bulk and monolayer ReS₂. We find that the low frequency rigid-layer vibration modes are nonexistent in this low symmetry bulk ReS₂ and due to the rather weak inter-layer interaction, the thickness induced frequency shifts are rather small and there is no surface reconstruction.. We believe combining with Raman measurement and LDA calculations is an efficient way for studying the vibrational and structural properties of 2D layered materials with low symmetry.

METHOD

Preparation of Single and Few-Layer ReS₂ Films. N type single crystals ReS₂ were obtained using Br₂ assisted chemical vapor transport method (more details in Tongay et al.'s paper¹⁵). We adopted the typical micromechanical exfoliation method to get few-layer ReS₂ flakes on Si

substrate with 300 nm SiO₂ by the visual color differences between samples and substrates. Using Zeiss microscope (Scope A1), we could identify the ReS₂ flakes, then determine their thickness by a AFM (Bruker, multimode 8).

Raman Spectroscopy. Raman experiments were performed using a 100x objective in a Horiba-JY T64000 system at ambient conditions. The excitation laser wavelength was 633 nm, with laser power kept as 1 mW and laser spot about 2 μ m in diameter. The backscattering geometry was adopted in Raman measurements, with spectrum resolution of 0.6 cm⁻¹. We took room temperature spectrum of every sample for 120s, and analyzed Raman peaks of the spectrum by the typical Lorentzian fitting procedure to get the corresponding Raman shift values.

Calculation Details. Brillouin zone center phonon frequencies calculations for few-layer NL (from 1L to 4L) including bulk ReS₂ were performed by the small displacement method. The calculations were performed in the framework of DFT, using the projector augmented wave (PAW)³⁵ method as implemented in the VASP code (Vienna ab-initio Simulation Package)^{36,37}. Different exchange-correlation functions such as the LDA scheme of Perdew and Zunger (CAPZ)³⁸ and the GGA schemes of Perdew-Burke (PB) and Perdew-Burke-Ernzerhof (PBE)³⁹ and Perdew-Wang 91 (PW91)⁴⁰ were tested. And the results of the LDA and the best GGA-PW91 were listed in the text. Since ReS₂ is a layered structure material that binds through vdW interaction between the layers. Therefore, to check the influence of vdW, we also included the vdW-corrected functions (vdW-DFT), Grimme corrections⁴¹ to PBE in the theoretical calculations and listed the results in the text. The basis set cutoff for the wave functions was 550 eV. The few-layer ReS₂ were simulated with a vacuum of 15 Å in the x direction to ensure negligible interaction between their periodic images. The Brillouin-zone integration was done on uniform Monkhorst-Pack grids of 1 * 24 * 24 for few-layer ReS₂ and 24 * 24 * 24 for bulk ReS₂.

The convergence criterion of self-consistent calculations for ionic relaxations was 10^{-5} eV between two consecutive steps. The internal coordinates and lattice constants were relaxed with full relaxation method for bulk ReS_2 . For few-layer ReS_2 , we relaxed the internal coordinates and lattice constants with fixing volume method to avoid the collapse of vacuum. The convergence criterion of relaxation was that the pressures on the lattice unit cell were less than 0.5 kBar and the Hellman-Feynman forces on the ions were less than 0.001 eV/Å.

Figure 1. (Color online) (a) A typical microscopic image of monolayer (in the red circle) and multilayer ReS_2 flakes on Si substrate with 300 nm thick SiO_2 . (b) An AFM image of the monolayer ReS_2 flake in the red circle of (a). Insert: the height probe profile of the monolayer ReS_2 , showing the monolayer ReS_2 height of 0.742 nm. (c) The lattice structure of bulk ReS_2 . Left figure, primitive cell of bulk ReS_2 perspective drawing down the interlayer lattice vector a . The vector b and c are in-plane lattice vectors. Right figure, periodical lattice structure of bulk ReS_2 . The parallelepiped is the primitive cell of bulk ReS_2 .

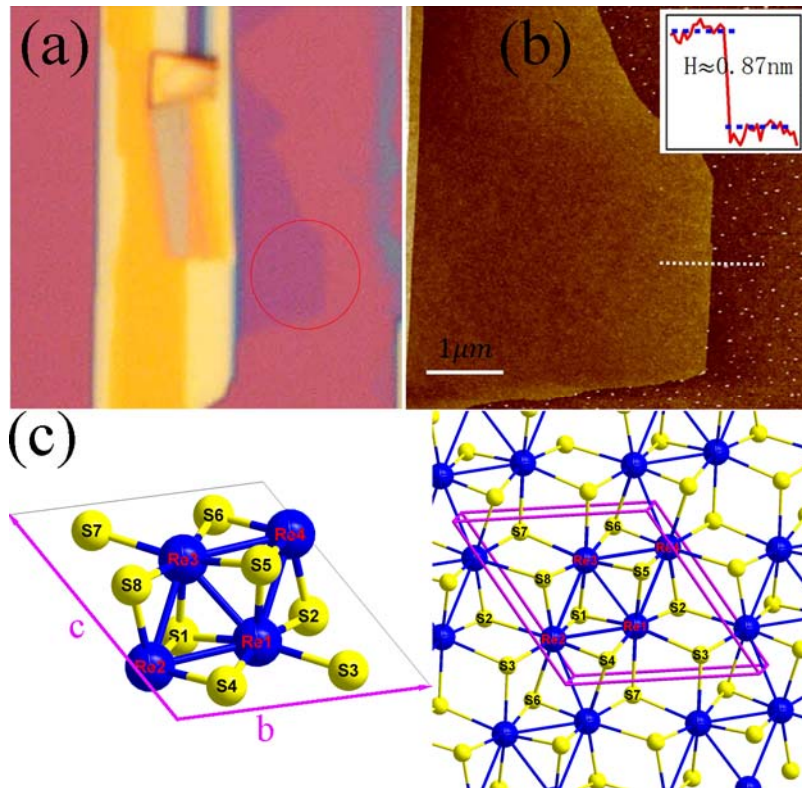


Figure 2. (a) Raman spectrum of bulk ReS_2 . The arrows mark the concrete positions of 18 Raman active modes of bulk ReS_2 . (b) Raman spectra of few-layer ReS_2 . The arrows mark the concrete positions of 18 Raman active modes of monolayer ReS_2 .

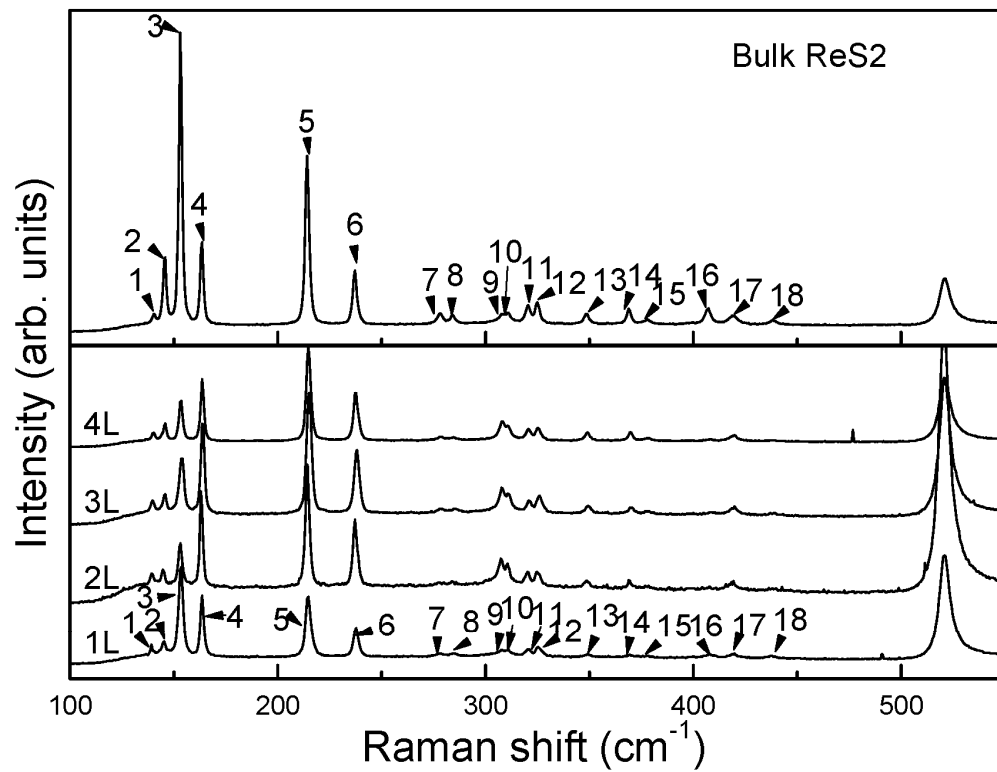


Figure 3. (Color online) Four E_g -like vibration modes at 153.6, 163.4, 218.2, 238.1 cm^{-1} and two A_g -like vibration at 136.8 and 144.5 cm^{-1} for bulk ReS_2 , from LDA theoretical calculations and analysis of the vibration eigenvectors. The lengths of the arrows are proportional to the modular of the phonon eigenvectors with the length weights less than 15 percentage ignored.

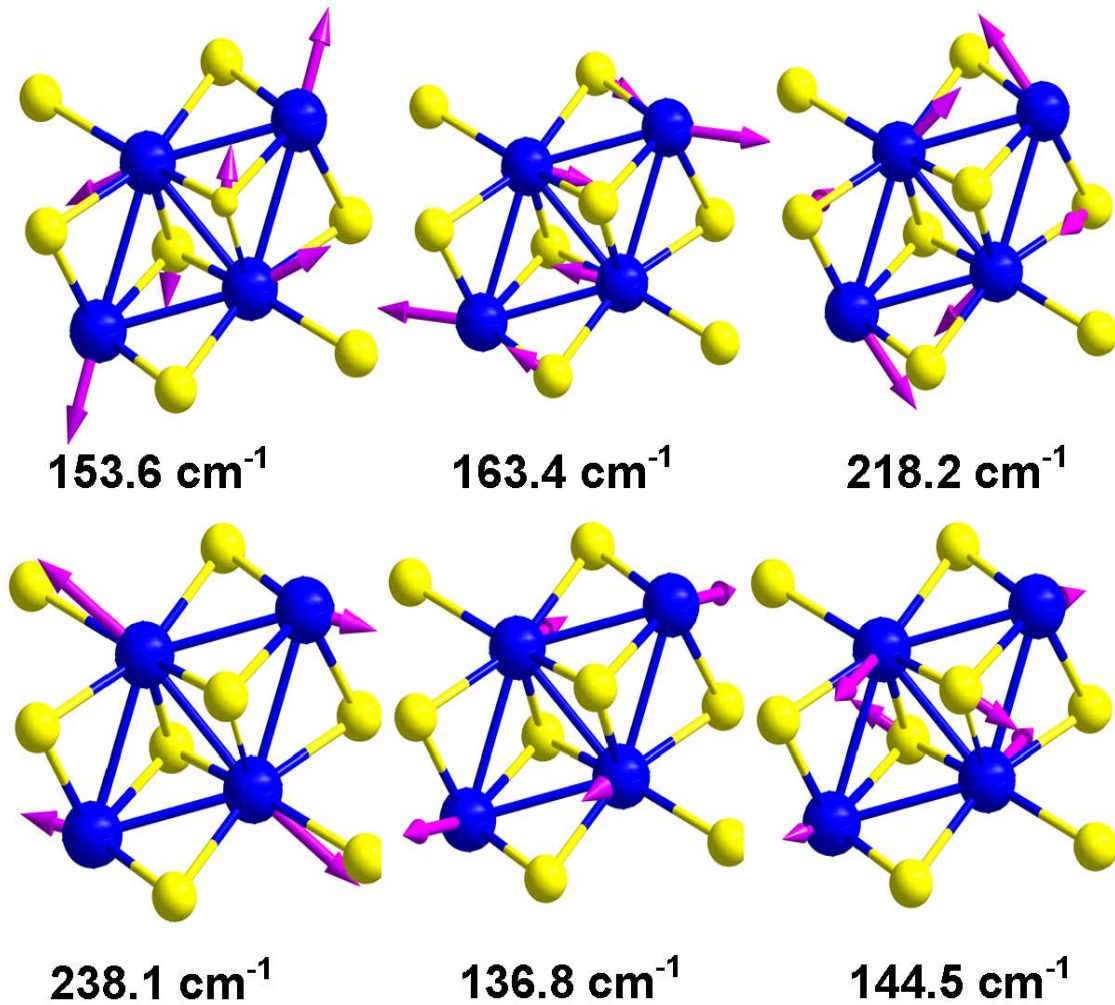


Table 1. The relaxed lattice parameters and independent fractional coordinates of bulk ReS₂ with DFT-LDA, vdW-DFT and DFT-GGA methods. The experimental data¹⁶ are listed for comparison. The lengths are in units of Å.

Lattice parameter	a		b	c	α	β	γ
LDA	6.315		6.482	6.415	121.4°	88.3°	106.6°
vdW-DFT	6.308		6.482	6.414	121.4°	88.3°	106.6°
GGA	7.389		6.588	6.527	121.3°	88.1°	105.0°
Exp. ¹⁶	6.417		6.510	6.461	121.1°	88.4°	106.5°
Fractional coordinates	bulk	Re1	Re2	S1	S2	S3	S4
x	LDA	0.503	0.492	0.210	0.276	0.696	0.761
	vdW-DFT	0.503	0.492	0.209	0.276	0.697	0.761
	GGA	0.502	0.492	0.252	0.309	0.667	0.722
	Exp. ¹⁶	0.503	0.493	0.217	0.277	0.698	0.756
y	LDA	0.513	0.058	0.250	0.774	0.754	0.279
	vdW-DFT	0.513	0.058	0.250	0.774	0.755	0.279
	GGA	0.512	0.058	0.262	0.783	0.746	0.266
	Exp. ¹⁶	0.511	0.056	0.250	0.771	0.753	0.273
z	LDA	0.298	0.247	0.366	0.383	0.119	0.119
	vdW-DFT	0.298	0.247	0.366	0.383	0.119	0.119
	GGA	0.298	0.247	0.374	0.390	0.114	0.115
	Exp. ¹⁶	0.297	0.248	0.368	0.384	0.117	0.118

Table 2. The relaxed independent Re-Re bond lengths (the lengths of Re2-Re3 and Re3-Re4 equate to Re1-Re4 and Re1-Re2, respectively a result of inversion symmetry) given by DFT-LDA, vdW-DFT and DFT-GGA methods. The experimental data¹⁶ are listed for comparison. The lengths are in units of Å.

Re-Re distance	Re1-Re2	Re1-Re3	Re1-Re4
LDA	2.77	2.68	2.78
vdW-DFT	2.77	2.68	2.78
GGA	2.82	2.72	2.84
Exp. ¹⁶	2.79	2.69	2.82

Table 3. The 18 Raman active frequencies (in units of cm^{-1}) in bulk ReS_2 of experimental measurement under 633 nm solid state excitation wavelength laser and first-principles theoretical calculations. The A_g -like, E_g -like and cp modes are also marked correspondingly.

Exp.	bulk	140.3	145.9	153.1	163.6	217.2	237.1
		278.3	284.2	307.8	311.0	320.6	324.9
		348.8	368.9	377.9	407.3	418.7	438.0
Exp.	1L	139.2	145.3	153.6	163.6	217.7	237.7
		278.3	284.7	307.8	311.0	320.6	324.9
		348.8	369.5	377.4	408.3	419.3	437.5
LDA	bulk	136.8	144.5	153.6	163.4	218.2	238.1
		(A_g like)	(A_g like)	(E_g like)	(E_g like)	(E_g like)	(E_g like)
		275.1	282.6	308.5	312.1	318.3	325.8
vdW-DFT	bulk	(cp)	(cp)	(E_g like)	(E_g like)	(cp)	(cp)
		349.7	370.4	381.3	408.7	422.3	443.4
		(cp)	(cp)	(cp)	(cp)	(A_g like)	(A_g like)
GGA	bulk	129.4	137.1	148.0	158.4	208.7	228.4
		261.5	268.5	295.8	298.3	303.2	311.1
		332.4	354.5	363.0	393.4	406.7	425.1
LDA	1L	132.7	142.4	155.5	164.3	220.2	241.3
		275.6	282.8	309.6	311.8	317.4	326.9
		350.4	371.6	380.3	410.8	423.8	443.7
GGA	1L	129.3	137.2	148.3	158.4	208.9	228.7

		261.9	268.8	295.9	298.2	303.5	311.1
		332.7	354.7	363.3	393.5	406.8	424.7

Table 4. The relaxed lattice parameter of monolayer ReS₂ with DFT-LDA and DFT-GGA methods. The VASP GGA-PBE results by Tongay et al.¹⁵ and Horzum et al.³³ are listed for comparison. The lengths are in units of Å.

Lattice parameter	a	b	c	α	β	γ
LDA	-	6.477	6.408	121.4°	88.1°	106.2°
GGA	-	6.587	6.526	121.3°	88.1°	107.0°
GGA ¹⁵	-	6.51	6.41	-	-	-
GGA ³³	-	6.51	6.40	-	-	-

AUTHOR INFORMATION

Corresponding Author

Correspondence and requests for materials should be addressed to F. M. (email: miao@nju.edu.cn), B. W. (email: bgwang@nju.edu.cn) or to X. W. (email: xgwan@nju.edu.cn).

Author Contributions

The manuscript was written through contributions of all authors. All authors have given approval to the final version of the manuscript. Yanqing Feng and Wei Zhou: these authors contributed equally.

ACKNOWLEDGMENT

The work is supported by the National Key Project for Basic Research of China (Grants No. 2011CB922101, 2015CB921600, 2013CBA01603), the National Natural Science Foundation of China (Grants No. 91122035, 11374142, 11174124, 11374147, 11474150), the Natural Science Foundation of Jiangsu Province (BK20130544, BK20140017), the Specialized Research Fund for the Doctoral Program of Higher Education (20130091120040), and Fundamental Research Funds for the Central Universities. H. T. Y. was supported by the Department of Energy, Office of Basic Energy Sciences, Division of Materials Sciences and Engineering, under contract DE-AC02-76SF00515. The project is also funded by Priority Academic Program Development of Jiangsu Higher Education Institutions. We also acknowledge the support for the computational resources by the High Performance Computing Center of Nanjing University.

REFERENCES

- 1 Novoselov, K.S.; Jiang, D.; Schedin, F.; Booth, T.J.; Khotkevich, V.V.; Morozov, S.V.; Geim, A.K. Two-Dimensional Atomic Crystals. *Proc. Natl. Acad. Sci. U.S.A.* 2005, 102, 10451-10453.
- 2 Castro Neto, A.H.; Guinea, F.; Peres, N.M.R.; Novoselov, K.S.; Geim, A.K. The Electronic Properties of graphene. *Rev. Mod. Phys.* 2009, 81, 109-162.
- 3 Chhowalla, M.; Shin, H.S.; Eda, G.; Li, L.J.; Loh, K.P.; Zhang, H. The Chemistry of Two-Dimensional Layered Transition Metal Dichalcogenide Nanosheets. *Nat. Chem.* 2013, 5, 263-275.
- 4 Wolverson, D.; Crampin, S.; Kazemi, A.S.; Ilie, A.; Bending, S.J. Raman Spectra of Monolayer, Few-Layer, and Bulk ReSe₂: An Anisotropic Layered Semiconductor. *ACS Nano* 2014, 10, 1021-1033.
- 5 Sander, T.; Eisermann, S.; Meyer, B.K.; Klar, P.J. Raman Tensor Elements of Wurtzite ZnO. *Phys. Rev. B* 2012, 85, 165208-165214.
- 6 Luo, X.; Zhao, Y.Y.; Zhang, J.; Toh, M.; Kloc, C.; Xiong, Q.H.; Quek, S.Y. Effects of Lower Symmetry and Dimensionality on Raman Spectra in Two-Dimensional WSe₂. *Phys. Rev. B* 2013, 88, 195313-195320.
- 7 Ferrari, A.C. Raman Spectrum of Graphene and Graphite: Disorder, Electron-Phonon Coupling, Doping and Nonadiabatic Effects. *Solid State Commun.* 2007, 143, 47-57.
- 8 Lee, C.; Yan, H.; Brus, L.E.; Heinz, T.F.; Hone, J.; Ryu, S. Anomalous Lattice Vibrations of Single- and Few-Layer MoS₂. *ACS Nano* 2010, 4, 2695-2700.
- 9 Ferrari, A.C.; Meyer, J.C.; Scardaci, V.; Casiraghi, C.; Lazzeri, M.; Mauri, F.; Piscanec, S.; Jiang, D.; Novoselov, K.S.; Roth, S.; Geim, A.K. Raman Spectrum of Graphene and Graphene Layers. *Phys. Rev. Lett.* 2006, 97, 18740.

- 10 Tan, P.H.; Han, W.P.; Zhao, W.J.; Wu, Z.H.; Chang, K.; Wang, H.; Wang, Y.F.; Bonini, N.; Marzari, N.; Pugno, N.; Savini, G.; Lombardo, A.; Ferrari, A.C. The Shear Mode of Multilayer Graphene. *Nat. Mater.* 2012, 11, 294-300.
- 11 Lui, C.H.; Leandro, M.M.; Kim, S.H.; Lantz, G.; Laverge, F.E.; Saito, R.; Heinz, T.F. Observation of Layer-Breathing Mode Vibrations in Few-Layer Graphene through Combination Raman Scattering. *Nano Lett.* 2012, 12, 5539-5544.
- 12 Zhao, Y.Y.; Luo, X.; Li, H.; Zhang, J.; Araujo, P.T.; Gan, C.K.; Wu, J.; Zhang, H.; Quek, S.Y.; Dreaaelhause, M.S.; Xiong, Q.H. Interlayer Breathing and Shear Modes in Few-Trilayer MoS₂ and WSe₂. *Nano Lett.* 2013, 13, 1007-1015.
- 13 Verble, J.L.; Wieting, T.J. Lattice Mode Degeneracy in MoS₂ and Other Layer Compounds. *Phys. Rev. Lett.* 1970, 25, 362.
- 14 Zeng, H.L.; Zhu, B.; Liu, K.; Fan, J.H.; Cui, X.D.; Zhang, Q.M. Low-Frequency Raman Modes and Electronic Excitations in Atomically Thin MoS₂ Films. *Phys. Rev. B* 2012, 86, 241301(R).
- 15 Tongay, S.; Sahin, H.; Ko, C.; Luce, A.; Fan, W.; Liu, K.; Zhou, J.; Huang, Y.; Ho, C.; Yan, J. Monolayer Behaviour in Bulk ReS₂ Due to Electronic and Vibrational Decoupling. *Nat. Commun.* 2014, 5, 3252-3258.
- 16 Murray, H.H.; Kelty, S.P.; Cbianelli, R.R. Structure of Rhenium Disulfide. *Inorg. Chem.* 1994, 33, 4418-4420.
- 17 Kelty, S.P.; Ruppert, A.F.; Cbianelli, R.R.; Ren, J.; Whangbo, M.-H. Scanning Probe Microscopy Study of Layered Dichalcogenide ReS₂. *J. Am. Chem. Soc.* 1994, 116, 7857-7863.
- 18 Lamfers, H.J.; Meetsma, A.; Wiegers, G.A.; de Boer, J.L. The Crystal Structure of Some Rhenium and Technetium Dichalcogenides. *J. Alloys Compd.* 1996, 241, 34-39.

- 19 Sanchez, A.M.; Wirtz, L. Phonons in Single-Layer and Few-Layer MoS₂ and WS₂. *Phys. Rev. B* 2011, 84, 155413-155420.
- 20 Luo, X.; Zhao, Y.Y.; Zhang, J.; Xiong, Q.H.; Quek, S.Y. Anomalous Frequency Trends in MoS₂ Thin Films Attributed to Surface Effects. *Phys. Rev. B* 2013, 88, 075320-075333.
- 21 Wilson, J.A. Modeling Contrasting Semimetallic Characters of TiS₂ and TiSe₂. *Phys. Status Solidi B* 1978, 86, 11-36.
- 22 Verble, J.L.; Wieting, T.J.; Reed, J.T. Rigid-Layer Lattice Vibrations and van der Waals Bonding in Hexagonal MoS₂. *Solid State Commun.* 1972, 11, 941-944.
- 23 He, J.-J.; Hummer, K.; Franchini, C. Stacking Effects on the Electronic and Optical Properties of Bilayer Transition Metal Dichalcogenides MoS₂, MoSe₂, WS₂, and WSe₂. *Phys. Rev. B* 2014, 89, 075409-075420.
- 24 Srivastava, S.K.; Avasthi, B.N. Review Layer Type Tungsten Dichalcogenide Compounds: Their Preparation, Structure, Properties and Uses. *J. Mater. Sci. Lett.* 1985, 20, 3801-3815.
- 25 Dresselhaus, M.S.; Dresselhaus, G.; Jorio, A. *Group Theory: Application to the Physics of Condensed Matter* (Springer, Berlin, Heidelberg, 1986).
- 26 Chen, S.H. Group-Theoretical Analysis of Lattice Vibrations in Metallic β -Sn. *Phys. Rev.* 1967, 163, 532-546.
- 27 Kresse, G.; Furthmüller, J.; Hafner, J. Ab initio Force Constant Approach to Phonon Dispersion Relations of Diamond and Graphite. *Europhys. Lett.* 1995, 32, 729-734.
- 28 Kern, G.; Kresse, G.; Hafner, J. Ab initio Calculation of the Lattice Dynamics and Phase Diagram of Boron Nitride. *Phys. Rev. B* 1999, 59, 8551-8559.

- 29 Serrano, J.; Bosak, A.; Arenal, R.; Krisch, M.; Watanabe, K.; Taniguchi, T.; Kanda, H.; Rubio, A.; Wirtz, L. Vibrational Properties of Hexagonal Boron Nitride: Inelastic X-Ray Scattering and Ab Initio Calculations. *Phys. Rev. Lett.* 2007, 98, 095503.
- 30 Fang, C.M.; Wiegers, G.A.; Haas, C.; de Groot, R.A. Electronic Structures of ReS₂, ReSe₂ and TcS₂ in the Real and the Hypothetical Undistorted Structures. *J. Phys.: Condens. Matter* 1997, 9, 4411-4424.
- 31 Michel, K.H.; Verberck, B. Theory of Rigid-Plane Phonon Modes in Layered Crystals. *Phys. Rev. B* 2012, 85, 094303-094314.
- 32 Geick, R.; Perry, C.H.; Rupprecht, G. Normal Modes in Hexagonal Boron Nitride. *Phys. Rev.* 1996, 146, 543-547.
- 33 Horzum, S.; Cakir, D.; Suh, J.; Tongay, S.; Huang Y.-S.; Ho, C.-H.; Wu, J.; Sahin, H.; Peeters, F.M. Formation and Stability of Point Defects in Monolayer Rhenium Disulfide. *Phys. Rev. B* 2014, 89, 155433-155440.
- 34 Mrstik, B.J.; Kaplan, R.; Reinecke, T.L. Surface-Structure Determination of the Layered Compounds MoS₂ and NbSe₂ by Low-Energy Electron Diffraction. *Phys. Rev. B* 1977, 15, 897-900.
- 35 Kresse, G.; Joubert, D. From Ultrasoft Pseudopotentials to the Projector Augmented-Wave Method. *Phys. Rev. B* 1999, 59, 1758-1775.
- 36 Kresse, G.; Hafner, J. Ab Initio Molecular Dynamics for Liquid Metals. *Phys. Rev. B* 1993, 47, 558-561.
- 37 Kresse, G.; Furthmüller, J. Efficient Iterative Schemes for Ab Initio Total Energy Calculations Using a Plane-Wave Basis Set. *Phys. Rev. B* 1996, 54, 11169-11186.

- 38 Perdew, J.P.; Zunger, A. Self-Interaction Correction to Density-Functional Approximations for Many-Electron Systems. *Phys. Rev. B* 1981, 23, 5048-5058.
- 39 Perdew, J.P.; Burke, K.; Ernzerhof, M. Generalized Gradient Approximation Made Simple. *Phys. Rev. Lett.* 1996, 77, 3865.
- 40 Perdew, J.P.; Wang, Y. Accurate and Simple Analytic Representation of the Electron-Gas Correlation Energy. *Phys. Rev. B* 1992, 45, 13244-13249.
- 41 Grimme, S. Semiempirical GGA-Type Density Functional Constructed with a Long-Range Dispersion Correction. *J. Comp. Chem.* 2006, 27, 1787-1799.